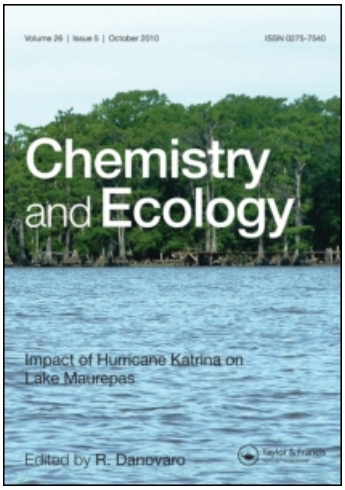

Chemistry and Ecology
Publication details, including instructions for authors and subscription information:
http://www.informaworld.com/smpp/title~content=t713455114

Deep chlorophyll maximum distribution in the central Tyrrhenian Sea described by a towed undulating vehicle

M. Marcelli[a]; M. Caburazzi[b]; A. Perilli[c]; V. Piermattei[a]; E. Fresi[b]
[a] DECOS, University of Tuscia, Viterbo, Italy [b] Dipartimento di Biologia (LESA), University of Roma 'Tor Vergata', Rome [c] Loc. Sa Mardini, CNR-IAMC Sez. Oristano, Torregrande-Oristano, Italy

To cite this Article Marcelli, M. , Caburazzi, M. , Perilli, A. , Piermattei, V. and Fresi, E.(2005) 'Deep chlorophyll maximum distribution in the central Tyrrhenian Sea described by a towed undulating vehicle', Chemistry and Ecology, 21: 5, 351 — 367
To link to this Article: DOI: 10.1080/02757540500290248
URL: http://dx.doi.org/10.1080/02757540500290248

Chemistry and Ecology
Vol. 21, No. 5, October 2005, 351–367

Taylor & Francis
Taylor & Francis Group

Deep chlorophyll maximum distribution in the central Tyrrhenian Sea described by a towed undulating vehicle

M. MARCELLI*†, M. CABURAZZI‡, A. PERILLI§, V. PIERMATTEI† and E. FRESI‡

†University of Tuscia, DECOS, via S. Giovanni Decollato 1, 01100, Viterbo, Italy
‡University of Roma 'Tor Vergata', Dipartimento di Biologia (LESA), via di Passo Lombardo 430, 00133 Rome
§CNR-IAMC Sez. Oristano, Loc. Sa Mardini, 09070, Torregrande-Oristano, Italy

(Received 3 March 2005; in final form 4 August 2005)

The towed undulating vehicle (TUV), named SARAGO, was used for two fine-scale surveys between the Italian and the Sardinian coasts during the Astraea 2 cruise (6–7 and 26–27 September 1995), studying the deep chlorophyll maximum distribution. SARAGO sections identify a sub-surface doming with higher chlorophyll *a* and primary production concentrations in the upwelling area of a cyclonic gyre region, detected by sea-surface temperature images. In the first section, the cyclone presents a double doming, in density and salinity, with shallower and concentrated patches of chlorophyll *a* for about 2 miles. Twenty days later, the second section shows that the gyre changes shape and extension, showing a single doming with higher primary production and chlorophyll *a* concentrations, distributed over a large area of about 40 nautical miles. SARAGO allows analysis of this high-variability phenomenon (cyclonic gyre) and allows concentrated patches (2 nm) to be identified, thus proving the importance of TUVs in the study of mesoscale processes.

Keywords: DCM; Primary production; SARAGO; Towed vehicle

1. Introduction

During 1994 and 1995, several oceanographic surveys were carried out in the central Tyrrhenian Sea with the following aims: (1) to estimate the primary production in oligotrophyc systems during summer, when it is mainly confined to the deep euphotic zone [1, 2]; and (2) to analyse the relation between the deep chlorophyll maximum (DCM) and the main physical parameters of the water column, utilizing new research technologies.

The knowledge of distribution and processes concerning the chlorophyll biomass is important to validate marine ecosystems' primary production models. Moreover the monitoring of the marine environment, at the basin scale, needs instruments which allow, at the same time, a high resolution and synoptic view, particularly in the study of phytoplankton populations [3].

*Corresponding author. Fax: +39 0766 21372; Email: marcomarcell@tin.it

Chemistry and Ecology
ISSN 0275-7540 print/ISSN 1029-0370 online © 2005 Taylor & Francis
http://www.tandf.co.uk/journals
DOI: 10.1080/02757540500290248

The asynopticity of single-ship measurements, the traditional oceanography (CTD casts with a SBE 911 plus probe), is one of the principal causes of several unresolved problems in biological oceanography.

The physical and biological processes which cause plankton patchiness, a fundamental and continuing oceanographic problem, are not yet understood [4]. Single-ship measurements cannot address these problems because the spatial structures often evolve faster than the sampling times [4]. They are highly dynamic: 'In a turbulent environment, horizontal and vertical diffusion, ensure that space and time are interrelated, so the discussion of spatial and temporal scales cannot be separated' [5].

Modern oceanography has three main technologies to overcome such problems: remote sensing, autonomous underwater profilers [6, 7] and undulating towed vehicles. Remote sensing permits the best synoptic spatial observation [8, 9], but the low spatial and temporal resolution do not allow the observation of the third spatial dimension, depth [10]. Autonomous underwater gliders represent a new technology that can be used to investigate entire sections of ocean basins, but they are limited, because they move at a very slow speed (0.5 kn. vs. the 1–10 kn. tow speed of the TUV SARAGO) and consequently they are not as well suited for fine-scale surveys.

Undulating towed vehicles, also called 'tow-fish', yield a better spatial and temporal resolution and a good synopticity, shortening the time needed, compared with traditional oceanography.

Our data have been collected by means of a towed undulating vehicle called the SARAGO [11], fitted with a CTD and a fluorometer which followed sinusoidal trajectories through the water column. This kind of technology has been successfully employed mainly in the Atlantic Ocean [4, 10, 12–14], but this is the first time it has been used in the Tyrrhenian Sea. This kind of technology was not frequently used in the Mediterranean Sea, where mesoscale phenomena are dominant.

Data were collected in two wide longitudinal transects in the central Tyrrhenian Sea. The Tyrrhenian Sea is mainly characterized by two gyres: a cyclonic gyre in the north and an anti-cyclonic gyre in the south of Boniface Mouth [15–19]. The Boniface Mouth is located between Sardinia and Corsica. These gyres, generated by the north-west Mistral wind, which blows through Boniface with a strong curl, induce upwelling and downwelling, respectively, and induce the mixing of Levantine intermediate water with Tyrrhenian surface waters, which have a great influence on the hydrological features of the whole western Mediterranean Sea. These gyres are also important in enhancing the flux of nutrients from depth into the euphotic layer, increasing the primary production of the Tyrrhenian Sea [16, 20]. Moreover, there is a lack of information concerning the relations between biological and physical–chemical parameters in the Tyrrhenian Sea [20].

Two longitudinal tow-fish transects were realized with a delay of 20 d, in the same area. In this work, we evaluate the evolution of the gyre in 20 days and the differences between the physical and biological characteristics of this structure.

2. Materials and methods

The study area is located in the central Tyrrhenian Sea at about 41° N between the Italian and Sardinian coasts (figure 1).

Between 6 and 27 September 1995, the Astraea2 Cruise was carried out onboard the Italian Coastal Guard's *R/V Bannock* (CP451). A large surface eddy, 100 nm, was detected in NOAA sea-surface temperature (SST) images. The strategy of the cruise was to cross the eddy with a gap of 20 days to analyse the possible variations of shape and dimension.

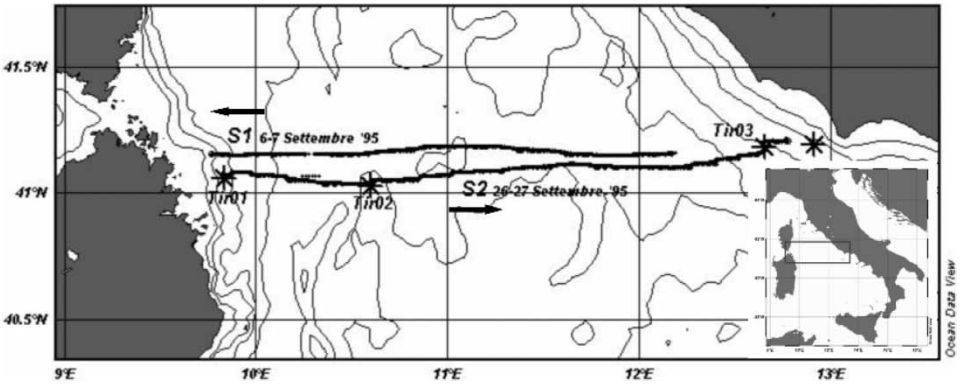

Figure 1. Study area.

The area was investigated using an underwater undulating towed vehicle, the SARAGO [21], along two longitudinal routes; satellite SST images; and hydrological and biological stations (figure 1).

The SARAGO is an underwater undulating vehicle with an external fibreglass vessel (figure 2), with a steel pressure hull inside containing the motor that controls the wings'

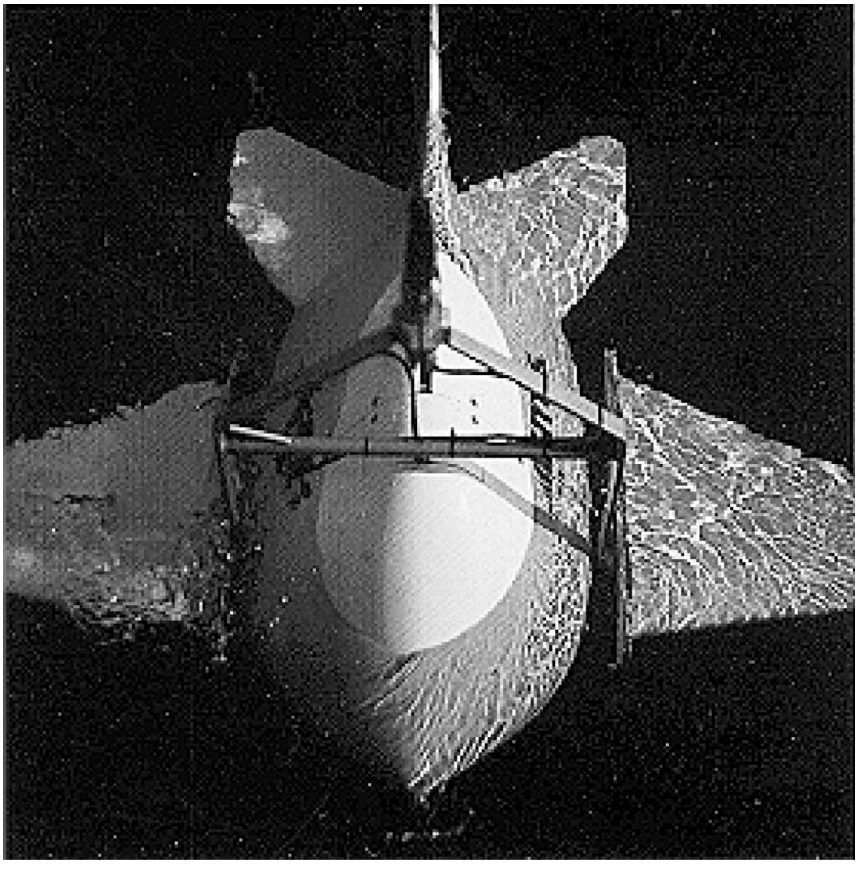

Figure 2. SARAGO towed undulating vehicle.

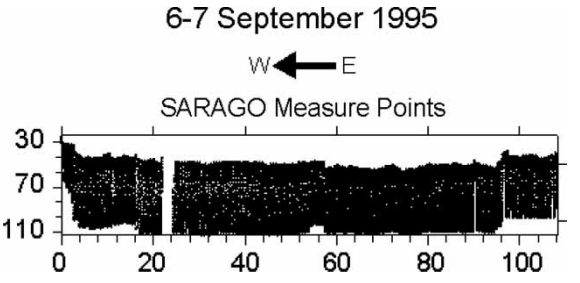

Figure 3. 6–7 September SARAGO measure points.

movement, trim control instruments, and the necessary electronic equipment for transmission of data and management of the tow fish. The measurement sensors and wings are connected to the pressure hull [11].

The SARAGO payload consists of a CTD (801 Idronaut) with temperature, pressure, conductibility, pH, Eh, and dissolved oxygen sensors and a fluorometer (Sea-tech FL0500).

An electro-mechanical cable connected to the ship helps visualize measured variables and trim control parameters. The data, together with the GPS ship position, are visualized and recorded by means of a personal computer.

With the SARAGO, it is possible to attain a high spatial resolution; in fact, we obtained a profile approximately every 350 m. In figures 3 and 4, we can see the trajectory carried out by SARAGO and, in figure 5, a zoom of the descent/ascent frequency of the vehicle.

Data collected by SARAGO were interpolated by the Kriging interpolation method, based on the linear variogram [22]. The interpolation of the values acquired along the two sinusoidal paths allowed the construction of the two sections discussed in this paper.

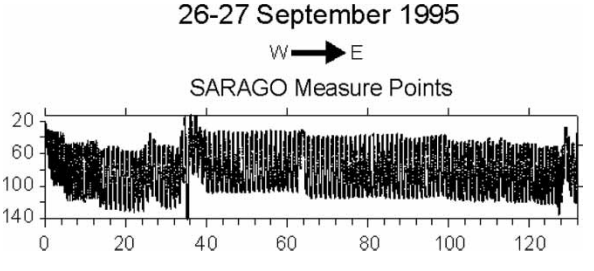

Figure 4. 26–27 September SARAGO measure points.

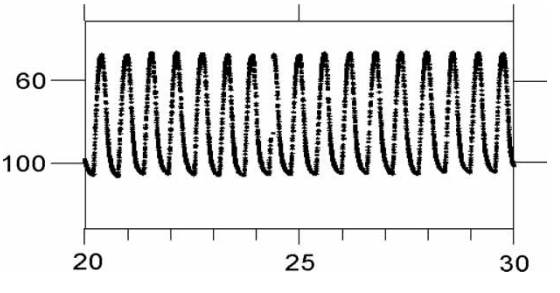

Figure 5. Example of the descent/ascent frequency of SARAGO.

During the survey, CTD casts and Primprod 1.08 profiles were performed, and water samples were collected for the instrument calibration.

The PrimProd 1.08 probe is a double impulse fluorometer, equipped with a PAR and a temperature sensor and a pressure transducer. This was developed at the Laboratory of Biophysics of the University of Moscow and works according to the 'pump and probe' method [23, 24]. This probe gives a quantitative measure of photochemical conversion efficiency. It is strictly related to the number of functional reaction centres of algae [25].

This measure is expressed from the ratio

$$\Delta\varphi_{\max} = F_v/F_{\max},$$

where $\Delta\varphi_{\max}$ is the photosynthetic efficiency and $F_v = F_{\max} - F_0$. The fluorescence $F_{\max}$ is measured after an impulse of high and saturating energy (pump), when all the reaction centres are closed.

The fluorescence F_0 is measured after a low-energy impulse (probe), when almost all the reaction centres are open, and the photochemical quenching is maximum. $\Delta\varphi_{\max}$ varies between 0 and 1.

From the measurements of biomass, PAR (photosynthetic active radiation) and $\Delta\varphi_{\max}$ it was possible to estimate the *in situ* primary production with the phyto VFP model [26, 27].

The model estimates the primary production for area units (mg C m^{-2} h^{-1}), by integration of the punctual values, from the surface to photic depth, the depth of the photic zone, calculated at 1% of the surface layer.

This simulates the *P–I* curve, subdividing the water column in three regions on the grounds of fixed PAR values, calculated experimentally. The first region represents the photo-limited area, which corresponds to the linear increase in primary production with light:

$$P = \phi \cdot a^* \cdot I \cdot \text{Chl } a \cdot \frac{F_v}{F_{\max}}.$$

The second region represents the photo-saturated area, where the production is constant:

$$P = \phi \cdot a^* \cdot E_k \cdot \text{Chl } a \cdot \frac{F_v}{F_{\max}}.$$

The third region represents the photo-inhibited area, which corresponds to the decrease in primary production in inverse proportion to light.

$$P = \frac{\phi \cdot a^* \cdot E_k \cdot E_I \cdot \text{Chl } a \cdot (F_v/F_{\max})}{I}.$$

P is the primary production; ϕ is the quantum yield of the photosynthetic process, 0,1 mol C per 10 mol photon, [28]; a^* is the specific absorption coefficient of the phytoplankton per mg chlorophyll a m^3, 0.016 m^2 per $mg_{\text{Chl}\,a}$, [29]; I is the irradiance (PAR); E_k is the maximum irradiance value, equivalent to the maximum photosynthetic efficiency; E_I is the irradiance value at the beginning of the photo-inhibition area.

The E_k and E_I values, utilized in the model for this work, were obtained using mean values by Kirk [28]. During this cruise, water samples were collected and analysed to calibrate our data; in fact, the model results were compared with primary production measures obtained by standard methods [30] (figure 6).

An SBE 911 plus CTD profiler was used in fixed stations to measure the hydrological variables (temperature, salinity, pressure, and density).

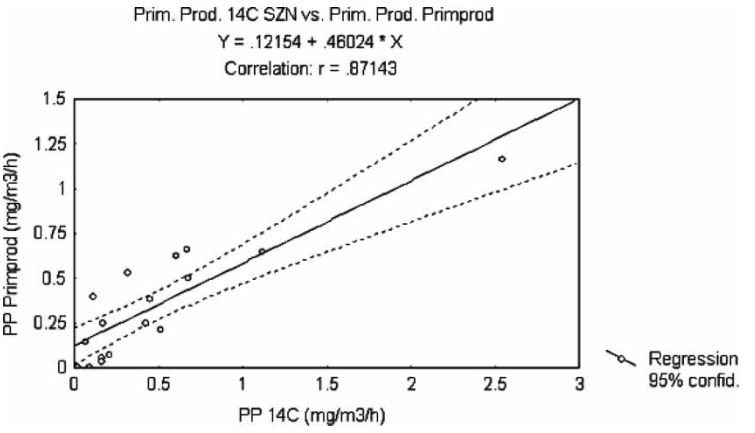

Figure 6. Comparison between primary production values measured by the 14C method and values estimated by the model based on Primrod 1.08 measurements.

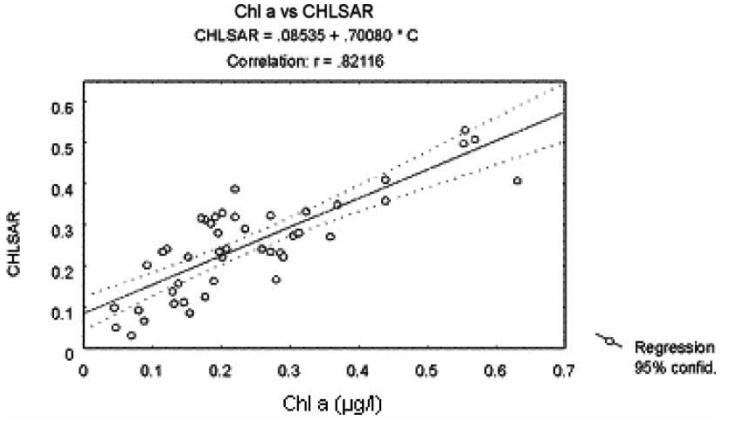

Figure 7. Correlation between chlorophyll *a* values measured with SARAGO and the results of an analysis carried out on samples collected at the same depth at which SARAGO carried out measurements.

At the same time, 40 samples of waters were collected in Niskin bottles to calibrate the fluorometers (figures 7 and 8). For each sample, 3 L of water was filtered with Whatman GF/F 47 mm filters. At the end of the cruise, filters were analysed by a standard spectrofluorometric technique to measure chlorophyll *a* [31].

Chlorophyll *a* measurements were used to calibrate SARAGO fluorimetric values (figure 7). The same method has been used to transform the Primprod 1.08 F_{max} measurements for chlorophyll *a* values (figure 8).

3. Results

3.1 *Satellite images*

We selected two SST images of the Tyrrhenian Sea: one represents the 7 September situation, the other the 27 September 1995 situation (figures 9 and 10). The black–blue colours indicate cold water, while the red–yellow colours indicate warm water.

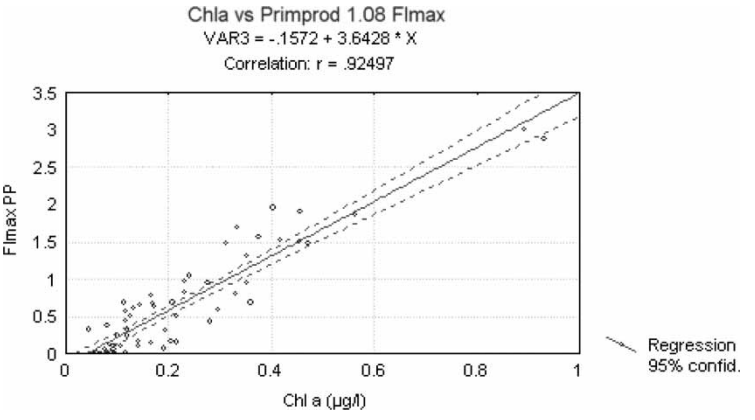

Figure 8. Calibration between Primprod 1.08 F_{max} and chlorophyll *a* measured by the spectroflurometer method.

The two tracks indicate the tow-fish paths: the east–west S1 (figure 9) and the west–east S2 (figure 10). The circles indicate the location of the Tir1, Tir2, Tir3, and Tir4 stations, along the route S2 (figure 10).

In the two SST images, a cyclonic gyre is identified in the northern Tyrrhenian Sea by colder water (figures 9 and 10). The shape and dimension of the cyclonic gyre changed significantly in 20 days.

In the 7 September image, the cyclonic gyre is mainly oriented from west to east. Colder water is detected upto the Sardinian coast. Presumably, the area was affected by a strong

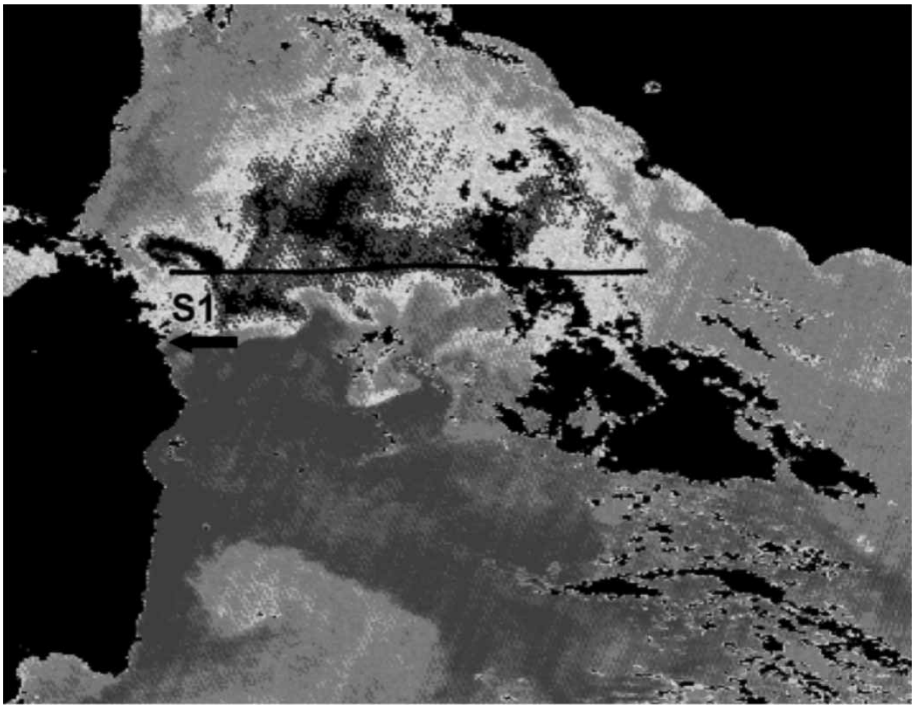

Figure 9. SST image of 6 September 1995.

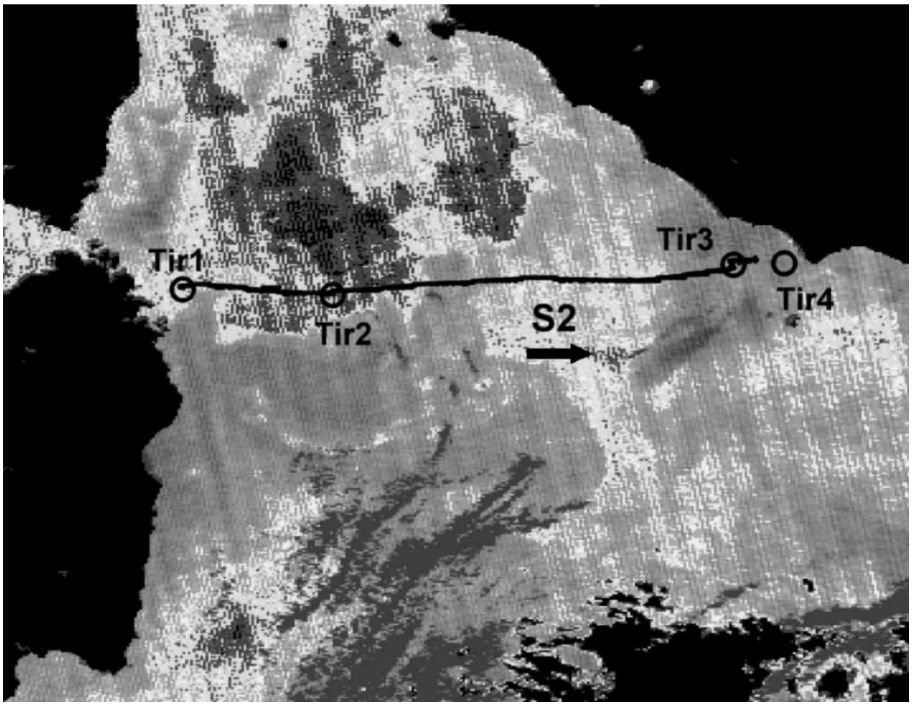

Figure 10. SST image of 27 September 1995.

mistral wind funnelled in the mountain around Olbia. In the western Tyrrhenian Sea, this wind blows perpendicularly to the coast and creates coastal upwelling and filaments [32].

In the 27 September image, the shape of the vortex is different, being larger and elongated toward the north.

3.2 *Hydrology*

The first SARAGO route (S1) was carried out from east to west, for 113 nautical miles, beginning on 6 September 1995 at 7.30 p.m. and finishing on 7 September 1995 at 2.30 p.m. It was mainly located inside the gyre and cut its core.

The second (S2) was carried out from west to east, for 133 nautical miles between 26 September 1995 at 11.15 p.m. and 27 September 1995 at 8.00 p.m.

The tow-fish section S2 cut the vortex in a more limited area, located on the southern part of the gyre.

The two hydrographical sections (figures 11 and 12) reflect the cyclonic gyre detected in the SST images. The cyclonic gyre is detected on the western side of both S1 and S2. In the two sections, between 25 and 120 m, the gyre is identified by doming of isopycnal (σ_t 28.8), isothermal (13.8 °C), and isohaline (38.3 PSU).

However, after 20 days, the shape and dimensions of the doming are different. An isopycnal of 28.8 and isohaline of 38.3 indicate a double doming in S1 and a single doming in S2.

The same isolines indicate that the doming is larger and shallower in S1 than in S2. At 80 m, colder (14 °C) and fresher water (38.15 PSU) is identified in the first 70 nautical miles in S1, and between the 20th and 60th nautical mile in S2.

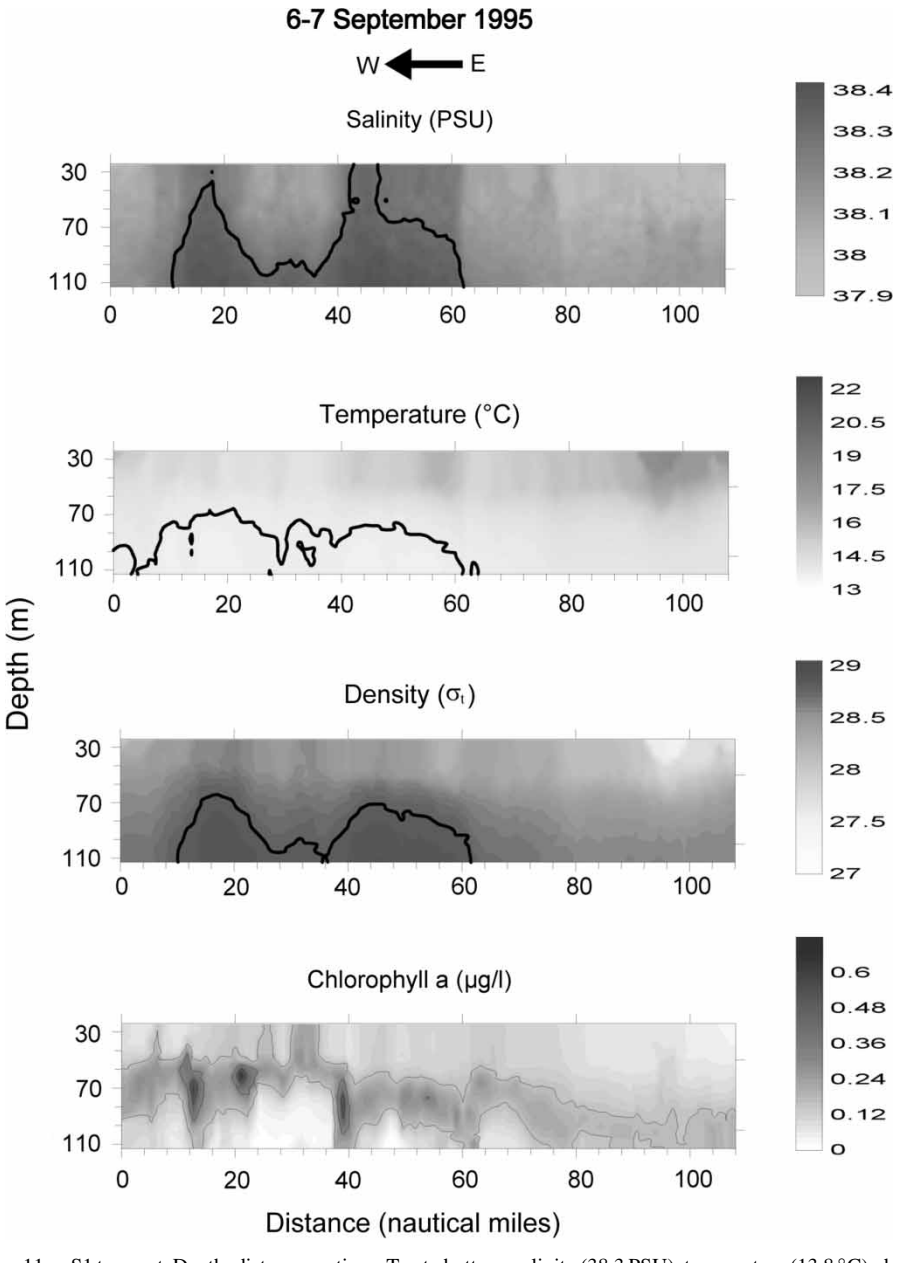

Figure 11. S1 transect. Depth–distance sections. Top to bottom: salinity (38.3 PSU); temperature (13.8 °C); density (σ_t 28.8); chlorophyll *a* ($\mu g\,L^{-1}$).

In the sections, the surface water of the area outside the gyre is identified by warmer and fresher waters. In particular, the temperature progressively increases toward the Italian peninsula.

During the survey, four hydrological and biological stations (Tir1, Tir2, Tir3, Tir4) were established, by means of Primprod 1.08, along S2: Tir1 was located on the continental shelf margin of the Sardinia coast; Tir2 was placed in the southern border of the cyclone; Tir3 was

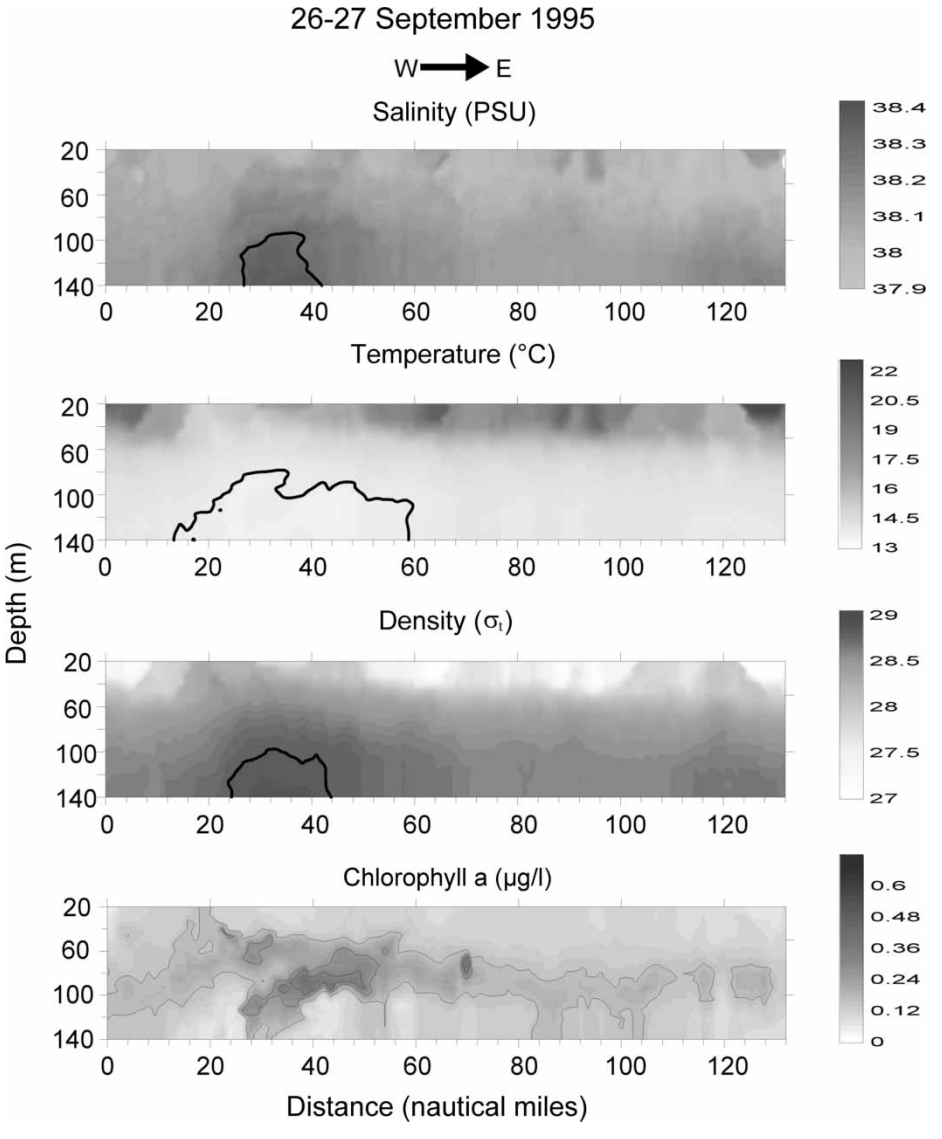

Figure 12. S2 transect. Depth–distance sections. Top to bottom: salinity (38.3 PSU); temperature (13.8 °C); density (σ_t 28.8); chlorophyll *a* ($\mu g\,L^{-1}$).

located on the continental shelf margin of the Italian peninsula; and Tir4 was placed on the Italian continental shelf (figure 10).

Colder water is only detected in the station Tir2. Warmer waters are present in the stations Tir 1, Tir3, and Tir4, located outside the gyre.

The temperature profiles of the PrimProd 1.08 stations (figure 13) show a well-defined mixed layer depth, which is shallower and colder in Tir2.

3.3 *Deep chlorophyll maximum*

The cyclonic gyre strongly influences the DCM distribution that, in the gyre core, is more intense and shallower. Both sections show a deepening of the DCM from west to east

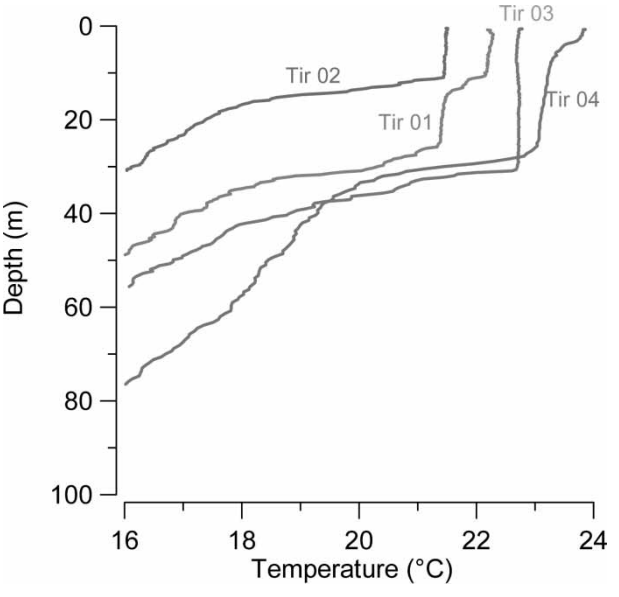

Figure 13. Temperature profile of the four stations in the upper layer.

(figures 11 and 12). However, there is a noticeable difference in the chlorophyll *a* distribution in the two sections.

In S1, inside the vortex, the chlorophyll *a* presents a patch distribution. There are three main patches of nearly 2 nm with a maximum concentration of about 0.7 $\mu g\,L^{-1}$ (figure 11). These are located in the first 40 miles, probably into the core of the vortex where the temperature is lower and the DCM is shallower (∼60 m). The integrated chlorophyll *a* between 40 and 110 m reflects the DCM distribution (figure 14).

The region between the two domings (between 20 and 40 nm) shows a chlorophyll *a*-depleted area where the integrated chlorophyll *a* shows the lowest values. On the eastern side of S1, the DCM progressively sinks until 100 m toward the Italian peninsula, and it is less intense and more uniformly distributed.

In the section S2, the cyclonic region is detected, between the 20th and 60th mile, by colder (∼13.7 °C) and fresher water (38.25 PSU). Inside the vortex, chlorophyll *a* is distributed more homogeneously than in S1, which is characterized by a patch distribution.

This area is characterized by a double DCM (figure 12). A first, shallower, and less concentrated, is detected, inside the gyre, about 60 m depth (figure 15), the same DCM depth of S1.

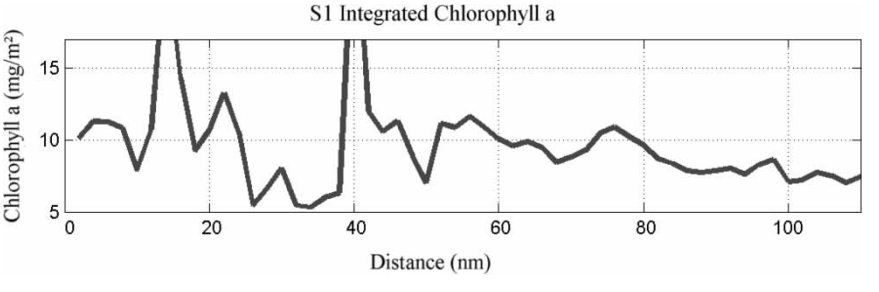

Figure 14. Chlorophyll *a* values integrated in the water column between 40 and 110 m depth.

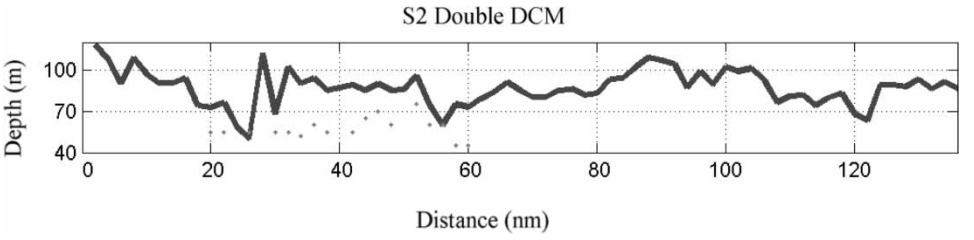

Figure 15. Depth DCM variation with distance.

A second, deeper, and more concentrated ($Chl_{max} = 0.45\,\mu\,g\,L^{-1}$), is detected at about 90 m. This is presumably due to a lateral intrusion of water because S2 cuts the southern part of the vortex, which should be a highly dynamic area. The gyre region, between the 20th and 60th mile, is characterized by a maximum of integrated chlorophyll *a*, which decreases toward the Italian peninsula where the cyclone is not present (figure 16).

The general pattern of chlorophyll *a* contours is strictly related to the hydrological parameters, particularly to the isopycnals of 28.8 and 28.7 (figure 17). Higher chlorophyll *a* values are observed where denser isopycnals are shoaling.

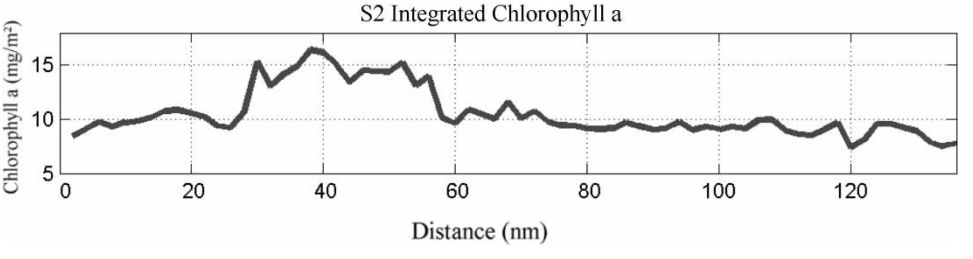

Figure 16. Chlorophyll *a* values integrated in the water column between 40 and 110 m depth.

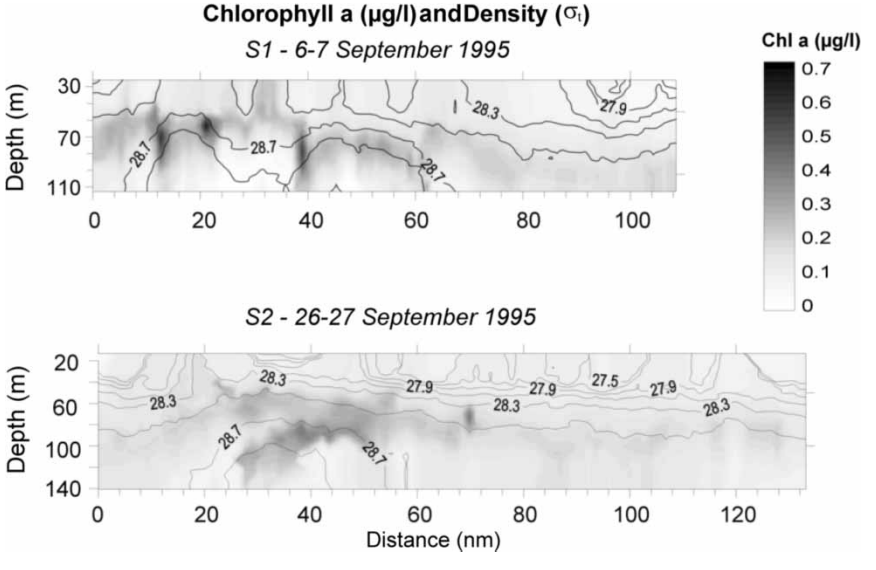

Figure 17. Isopycnals superimposed on the distribution of chlorophyll *a*.

3.4 *Primary production*

In order to compare the primary production, estimated at different times in the four Primprod 1.08 stations between 26 and 27 September, the PAR was standardized to a surface value of $1600\,\mu E\,m^{-2}\,s^{-1}$. In the four stations, primary production was estimated by the model, previously described, utilizing Primprod 1.08 chlorophyll *a*, PAR, and photosynthetic efficiency measures.

The depth, extension, and values of DCM are different in the four stations (figures 18 and 19): Tir1 DCM is 92 m deep with mean values of $0.3\,\mu g\,L^{-1}$; Tir2 shows a double DCM: the first 70 m deep ($0.32\,\mu g\,L^{-1}$) and the second extended between 95 m and 120 m ($0.42\,\mu g\,L^{-1}$); Tir3 DCM has lower values, $0.27\,\mu g\,L^{-1}$, at a depth of 90 m; Tir4 is located on the continental shelf, and its DCM, under 60 m, shows the lowest values ($0.20\,\mu g\,L^{-1}$). The general pattern that emerges is coherent with SARAGO data.

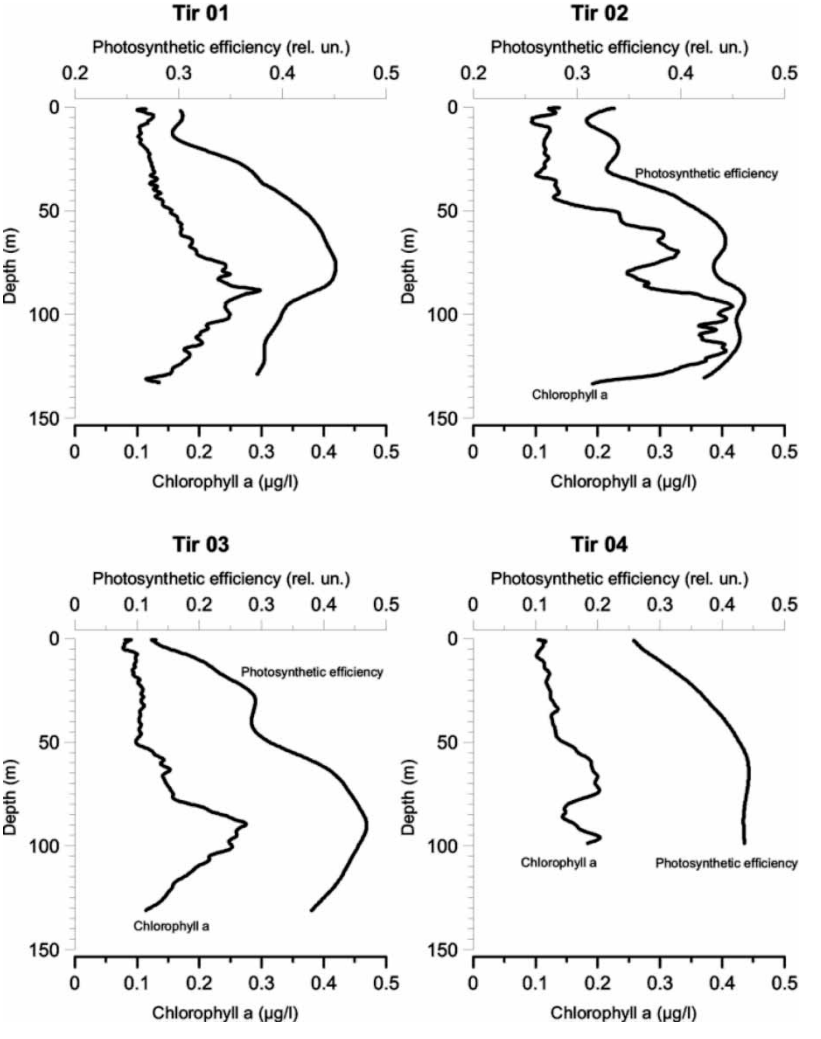

Figure 18. Chlorophyll *a* and photosynthetic efficiency profiles in the four stations.

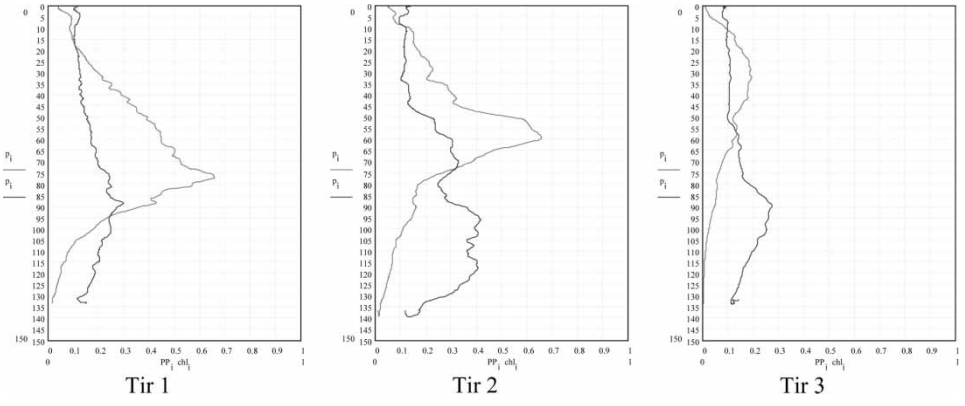

Figure 19. Chlorophyll *a* ($\mu g\,L^{-1}$), and primary production ($mg\,C\,m^{-2}\,h^{-1}$) profiles in the PrimProd stations.

The photosynthetic efficiency (F_v/F_{max}) shows minimum values in the upper layer (in the photoinhibition area), increases until the DCM depth, and below begins to decrease (figure 18).

The reduction may be due to the presence of chlorophyll degradation products and 'soluble fluorescence' [25, 33, 34], and senescence of cells [25].

An increase in photosynthetic efficiency from surface to DCM was already observed in some other cases, for example in the Sargasso Sea [34] and the north-east tropical Atlantic [25].

The photosynthetic efficiency highest values are in the upper portion of the DCM layer according to the ecology of phytoplankton at DCM. In the upper portion of DCM, functional cells are exposed to a higher light radiation, while senescent cells and chlorophyll degradation products are mainly in the lower portion [33, 35].

Primary production estimates, calculated from PrimProd data and represented by the primary production (red in online version of figure) profiles in figure 19 show maximum values some metres above the DCM, a situation described for other pelagic environments in the Mediterranean [2] and the oceans [36] (figure 19).

Table 1 lists the values of primary production in $mg\,C\,m^{-2}\,h^{-1}$, the chlorophyll *a* integrated into the water column between 40 and 110 m (for comparison with SARAGO data), and the photic depth at 1% of surface irradiance.

The highest integrated PP values are detected at stations Tir1 and Tir2, located on the border and inside the cyclonic gyre. The Tir3 and Tir4 stations, near the Italian peninsula, show the lowest values.

Unexpectedly, the primary production values are higher in Tir1 than in Tir2. This is probably due to a lower light penetration in Tir2 (80%) due to the upper DCM, which is responsible for the light attenuation in the photic layer, reducing the light availability for the deeper and more intense DCM.

Table 1. Primary production ($mg\,cm^{-2}\,h^{-1}$), chlorophyll *a* ($mg\,m^{-2}$) and photic depth (m) values of the PrimProd stations.

	PP ($mg\,C\,m^{-2}\,h^{-1}$)	Integrated values of Chl *a* ($mg\,m^{-2}$) between 40 and 110 m	Photic depth (1% surface irradiance)
Tir 1	33.457	14.429	102
Tir 2	29.5	20.624	80.7
Tir 3	13.729	12.494	66.07
Tir 4	15.926	10.211	65

4. Discussion and conclusion

The chlorophyll *a* distribution detected in the two Tyrrhenian Sea sections seems to have the same structures and intensity as those observed in different regions of Mediterranean Sea [2, 37, 38]. During the summer, in the oligotrophyc pelagic ecosystem, chlorophyll *a* is distributed in DCM [36, 39, 40] and has a very low concentration in the upper layer. The low nutrient concentration in the surface water is due to nutrient depletion by phytoplankton. The strong pycnocline, due to summer stratification, represents a barrier of vertical transport and limits fluxes of nutrients from deeper layers into the mixing layer. Below the mixing layer, chlorophyll *a* is distributed in DCM.

The cyclonic gyre influences the chlorophyll *a* distribution: the DCM is 10–20 m shallower, and the chlorophyll mean concentration is 0.05–0.1 $\mu g\, L^{-1}$ higher than in the rest of the transect. Intense patches of chlorophyll *a*, with concentrations of about 0.7 $\mu g\, L^{-1}$, are detected in denser and colder water. The shallower and more intense DCM seems to confirm that primary production is directly related to light and nutrients [2, 9, 41–43].

Beyond the cyclonic gyre, the chlorophyll is distributed in deep chlorophyll maximum at a depth of 90–110 m and is quite low. The mean concentrations are about 0.15–0.2 $\mu g\, L^{-1}$ in both sections.

The main differences between the two transects are distance, about 4′ of latitude, and evolution of dynamic phenomena during the time elapsed between the transects (20 d).

The SST images show a different shape and extension of the gyre. Therefore, we presume that these differences between the two transects are due to the evolution of the gyre. An oceanographic cruise has a period of about 20 d. These results indicate that the towed undulating vehicle better reproduces the mesoscale phenomena, because in 20 d these phenomena can significantly change.

With more detailed observation, an important difference emerges from the comparison between the hydrological parameters and the chlorophyll *a* distribution of the sections: (1) the intensity of the upwelling, detected by the doming of the isopycnals, $\sigma_t = 28.8$, is greater in transect S1 than in S2; (2) the S2 water column is more stratified and presents a sharp thermocline; (3) S1 presents a stronger patchiness distribution than S2, while in the external part of the gyre, the depth of the DCM and the chlorophyll *a* concentration are comparable.

From the PrimProd data, it is not possible to have a similarly high-resolution description of the area, but they do provide information about the ecology of the phytoplankton populations.

SARAGO data, Primprod data, and SST images, together with literature values on the variability of the circulation in this area [18, 19], indicate that the upwelling, under episodic strong wind events, modulates the distribution of the phytoplankton patchiness and enhances the primary production.

As soon as the upwelling episode ceases, or its intensity is reduced, phytoplankton can survive by recycling nutrients, and senescent cells and degradation products of chlorophyll appear.

The clear correspondence between SARAGO sections, SST images, and PrimProd stations profiles identifies the gyre area defined by colder water and lower stratification. The region outside the gyre is otherwise defined by a warm and stratified water, with a sharp thermocline.

Acknowledgements

The oceanographic cruises were carried out in agreement with Ismes S.p.A. and the Italian Coastal Guard with the aim of developing new technologies and methods for monitoring the Mediterranean Sea. We gratefully acknowledge support from Stefano Scarascia, Antonio Raimondi, Corrado Gaspani, and Gualtiero Baldi. Particular thanks goes to Luigi Lazzara for the useful suggestions.

References

[1] B.M. Jamart, D.F. Winter, K. Banse, G.C. Anderson, R.K. Lam. A theoretical study of phytoplankton growth and nutrient distribution in the Pacific Ocean off the north western U.S. coast. *Deep-Sea Res.*, **24**, 753–773 (1977).

[2] M. Estrada. Deep Phytoplankton and chlorophyll maxima in the Western Mediterranean. In *Mediterranean Marine Ecosystems, NATO Conference Series*, M. Moriartou-Apostolopoulou, V. Kiortsis (Eds), pp. 247–279, Plenum Press, New York (1985).

[3] T. Platt, S. Sathyendranath. Oceanic primary production: estimation by remote sensing at local and regional scales. *Science*, **241**, 1613–1620 (1988).

[4] M.A. Srokosz, A.P. Martin, M.J.R. Fasham. On the role of biological dynamics in plankton patchiness at the mesoscale: An example from the eastern North Atlantic Ocean. *J. Mar. Res.*, **61**, 517–537 (2003).

[5] G.P. Harris. Temporal and spatial scales in phytoplankton ecology. Mechanisms, methods, models, and managements. *Can. J. Fish. Aquat. Sci.*, **37**, 877–900 (1980).

[6] T.D. Dickey. Recent advances and future directions in multi-disciplinary in situ oceanographic measurements systems. In *Toward a Theory on Biological–Physical Interactions in the World Ocean, NATO ASI Series*, B.J. Rothschild (Ed.), pp. 555–599, Kluwer Academic, Dordrecht (1988).

[7] R. Williams. Evaluation of new techniques for monitoring and assessing the health of large marine ecosystems. In *Evaluating and Monitoring the Health of Large-Scale Ecosystems, NATO ASI Series 128*, D.J. Rapport, C.L. Gaudet, P. Calow (Eds), pp. 257–272, Springer, Berlin (1995).

[8] S.E. Lohrenz, R.A. Arnone, D.A. Wiesenburg, I.P. DePalma. Satellite detection of transient enhanced primary production in the western Mediterranean Sea. *Nature*, **335**, 245–247 (1988).

[9] K.U. Wolf, J.D. Woods. Lagrangian simulation of Primary Production in the physical environment—The Deep Chlorophyll Maximum and Nutricline. In *Toward a Theory on Biological–Physical Interactions in the World Ocean, NATO ASI Series*, B.J. Rothschild (Ed.), pp. 51–71, Kluwer Academic, Dordrecht (1988).

[10] V.H. Strass, J.D. Woods. Horizontal and seasonal variation of density and chlorophyll profiles between Azores and Greenland. In *Toward a Theory on Biological–Physical Interactions in the World Ocean, NATO ASI Series*, B.J. Rothschild (Ed.), pp. 113–137, Kluwer Academic, Dordrecht (1988).

[11] M. Marcelli, E. Fresi. 'The SARAGO' project: new undulating towed vehicle for developing, testing new technologies for marine research and environmental monitoring. *Sea Technol.*, **July**, 62–67 (1997).

[12] M.J.R. Fasham, T. Platt, B. Irwin, K. Jones. Factors affecting the spatial pattern of the deep chlorophyll maximum in the region of the Azores Front. *Prog. Oceanog.*, **14**, 129–165 (1985).

[13] V.H. Strass, J.D. Woods. New production in the summer revealed by the meridional slope of the deep chlorophyll maximum. *Deep-Sea Res.*, **38**(1), 35–56 (1991).

[14] V. Strass. Chlorophyll patchiness caused by mesoscale upwelling at fronts. *Deep-Sea Res.*, **39**(1), 75–96 (1992).

[15] J. Moen. *Variability and Mixing of the Surface Layer in the Tyrrhenian Sea: MILEX-80, Final Report, SACLANTCEN Rep. SR-75*, SACLANT Research Centre, La Spezia, Italy (1984).

[16] R. Nair, E. Cattini, G.P. Gasparini, G. Rossi. *Circolazione Ciclonica E Distribuzione Dei Nutrienti Nel Tirreno Settentrionale. Atti Del 10° Congresso AIOL*, pp. 65–76 (1992).

[17] D. Bacciola, M. Borghini, F. Dell'Amico, C. Galli, G.P. Gasparini, E. Lazzoni, G. Raso. *The TEMPO Experiment: TEMPO1 Hydrographic Campaign in the north Tyrrhenian Sea. 27 September to 7 October 1989, Data Report* (1993).

[18] V. Artale, M. Astraldi, G. Buffoni, G.P. Gasparini. Seasonal variability of gyre-scale circulation in the northern Tyrrhenian Sea. *J. Geophys. Res.*, **99**(C7), 14 127–14 137 (1994).

[19] M. Astraldi, G.P. Gasparini. The seasonal characteristics of the circulation in the Tyrrenian Sea. In *Seasonal and Interannual Variability of the Western Mediterranean Sea. Coastal and Estuarine Studies*, Vol. 46, pp. 115–134 (1994).

[20] G.C. Carrada, M. Ribera-D'Alcalà, V. Saggiomo. The pelagic system of the southern Tyrrhenian Sea. Some comments and working hypotheses. In *Atti del IX Congresso AIOL*, pp. 151–156 (1990).

[21] M. Marcelli, A. Perilli, A. Di Maio, S. Ziantoni. New operative methods to study pelagic ecosystems. *Operational Oceanography: Implementation at European and Regional Scales. Elsevier Oceanography Series 66, EuroGOOS Publication No. 17*, pp. 525–531, Elsevier Science, Amsterdam (2002).

[22] R. Barnes. The variogram sill and the sample variance. *Math. Geol.*, **23**, 673–678 (1991).

[23] P.G. Falkowski, K. Wyman, A.C. Ley, D.C. Mauzerall. Relationship of steady state photosynthesis to fluorescence in eucaryotic algae. *Biochim. Biophys. Acta*, **849**, 183 (1986).

[24] T.K. Antal, P.S. Venediktov, D.N. Matorin, M. Ostrowska, B. Wozniak, A.B. Rubin. Measurement of phytoplankton photosynthesis rate using a pump-and-probe fluorometer. *Oceanologia (Poland)*, **43**(3), 291–313 (2001).

[25] M. Babin, A. Morel, H. Claustre, A. Bricaud, Z. Kolber, P.G. Falkowski. Nitrogen and irradiance variations of the maximum quantum yeild of carbon fixation in eutrophic, mesotrophic and oligotrophic marine systems. *Deep-Sea Res.*, **43**(8), 1241–1272 (1996).

[26] M. Marcelli, O. Campana, A. Di Maio, O. Mangoni, M. Ribera D'Alcala', V. Saggiomo, S. Tozzi, E. Fresi. Development of a new operative method to estimate primary production in the pelagic system with a quasi synoptic space time scale, paper presented at Progress in oceanography of the Mediterranean sea—International Conference, Rome, 17–19 November 1997. Abstract volume, pp. 309–310 (1997).

[27] I. Nardello, L. Lazzara, M. Marcelli. Stime di biomassa e produzione primaria nel canale di Sicilia, attraverso misure di fluorescenza in vivo della clorofilla a, paper presented at Proceedings of XIII Congresso nazionale della Società Italiana di Ecologia, Vol. 27, p. S11.8 (2003).
[28] J.T.O. Kirk. *Light and Photosynthesis in Aquatic Ecosystems*, Cambridge University Press, Cambridge (1983).
[29] D. Antoine, A. Morel. Oceanic primary production, 1. Adaptation of a spectral light-photosynthesis model in view of application to satellite chlorophyll observations. *Global Biogeochem. Cycles*, **10**, 43–55 (1996).
[30] E. Steeman Nielsen. The use of radioactive carbon (14C) for measuring organic production in the sea. *J. Cons. Int. Explor. Mer.*, **18**, 117–140 (1952).
[31] L. Lazzara, F. Bianchi, M. Falcucci, V. Hull, M. Modigh, M. Ribera D'Alcala'. Pigmenti clorofilliani. *Nova Thalassia*, **11**, 207–235 (1990).
[32] A. Perilli, V. Rupolo, S.E. Salusti. Satellite investigations of a cyclonic gyre in Central Tyrrhenian Sea (Western Mediterranean Sea). *J. Geophys. Res.*, **100**, 2487–2499 (1995).
[33] A. Herbland. The soluble fluorescence in the open sea: distribution and ecological significance in the equatorial Atlantic Ocean. *J. Exp. Mar. Biol. Ecol.*, **32**, 275–284 (1978).
[34] J.R. Geider, R.M. Greene, Z. Kolber, H.L. MacIntyre, P.G. Falkowski. Fluorescence assessment of the maximum quantum efficiency of photosynthesis in the western North Atlantic. *Deep-Sea Res.*, **40**(6), 1205–1224 (1993).
[35] P.K. Bienfang, J. Szyper. Phytoplankton dynamics in the subtropical Pacific Ocean off Hawaii. *Deep-Sea Res.*, **28A**(9), 981–1000 (1981).
[36] J.J. Cullen. The deep chlorophyll maximum: comparing vertical profiles of chlorophyll a. *Can. J. Fish. Aquat. Sci.*, **39**, 791–803 (1982).
[37] R.A. Varela, A. Cruzado, J. Tintore, E.G. Ladona. Modelling the deep-chlorophyll maximum: A coupled biological–physical approach. *J. Mar. Res.*, **50**, 441–463 (1992).
[38] M. Delgado, M. Latasa, M. Estrada. Variability in the size-fractionated distribution of the phytoplankton across the Catalan front of the north-west Mediterranean. *J. Plank. Res.*, **14**(5), 753–77 (1992).
[39] E.L. Venrick, J.A. McGowan, A.W. Mantyla. Deep maxima of photosynthetic chlorophyll in the Pacific Ocean. *Fish. Bull.*, **71**(1), 41–52 (1973).
[40] E. Shulenberger, J. Reid. The Pacific sallow oxygen maximum, deep chlorophyll maximum, and primary productivity, reconsidered. *Deep-Sea Res.*, **28A**(9), 901–919 (1981).
[41] A. Herbland, B. Voituriez. Hydrological structure analysis for estimating the primary production in the tropical Atlantic Ocean. *J. Mar. Res.*, **37**, 87–101 (1979).
[42] J.J. Cullen, R.W. Eppley. Chlorophyll maximum layers of the Southern California Bight and possible mechanisms of their formation and maintenance. *Oceanol. Acta*, **4**(1), 23–32 (1981).
[43] M. Estrada, F. Vives, M. Alcaraz. Life and the productivity of the open sea. In *Western Mediterranean*, R. Margalef (Ed.), pp. 148–198, Pergamon Press, Oxford (1985).